AIAA JOURNAL
Vol. 41, No. 9, September 2003

Nonlinear Response of Aeroservoelastic Systems Using Discrete State-Space Approach

P. C. Chen* and E. Sulaeman†
ZONA Technology, Inc., Scottsdale, Arizona 85251-3540

A generalized direct simulation method using a discrete time-domain state-space approach for transient response of both open- and closed-loop nonlinear aeroelastic systems is developed. Based on a nonlinear parameter scheme that divides the nonlinear system into sublinear systems, the method first assembles a set of discrete time-domain state-space equations and then computes the transient response by switching the time-integration procedure between this set of state-space equations. In so doing, various nonlinearities in structures, aerodynamics and/or control systems can be included. The method is validated by correlating the transient response of a three-degree-of-freedom airfoil section in freeplay with the experimental and numerical results obtained by Conner et al. The stability of a strut-braced wing with buckling effects at two trim conditions is also studied, which shows that the aeroelastic stability of the present strut-braced wing is trim-condition dependent. Such results clearly could not be obtained if using a linear aeroelastic analysis.

I. Introduction

In the past, various techniques have been proposed by many investigators for predicting the transient response of aeroelastic systems that involves nonlinearities either in the structures or in the aerodynamics.[1–19] In general, these techniques can be classified into two categories: 1) the describing function or harmonic balance method and 2) the direct numerical simulation approach. The describing function method assumes that the nonlinear system admits a periodic solution dominated by the fundamental harmonic, that is, effects of higher harmonics are neglected. This gives an equivalent linear system that is then analyzed by conventional means, such as frequency-domain eigenanalysis. Lee[9] demonstrated that the describing function method could be extended to handle large dynamic systems with multiple structural nonlinearities. However, the describing function method is applicable only for concentrated nonlinearities such as freeplay in control surface actuation. For distributed nonlinearities such as large-amplitude aerodynamics, friction in riveted joints, etc., deriving expression of the equivalent linear systems becomes difficult.

The direct simulation approach assumes that the nonlinear system can be divided into several subdomains, and within each subdomain, the system, whose transient response can be computed by a straightforward time-integration procedure, is assumed to be linear. The overall response of the nonlinear system is then obtained by switching the time-integration procedure between subdomains. The only drawback of the direct simulation approach is that the quantitative measures of the stability characteristics of the system cannot be directly assessed without a proper postprocessing procedure.

In this paper, a generalized direct simulation method using a discrete time-domain state-space approach for both open- and closed-loop nonlinear aeroelastic systems is presented. This approach is based on a nonlinear parameter scheme that divides the nonlinear systems into sublinear systems, which leads to a set of piecewise discrete time-domain state-space equations. In so doing, nonlinearity in structures, control system, and unsteady aerodynamics can be included altogether. Either the discrete gust or pilot input commands can be specified as the external disturbance to excite the nonlinear system. The transient response is computed based on an interpolation procedure to obtain the state-space equations at each time step. Once the time-domain solution of the generalized coordinates is obtained, the transient response of any parameters of the aeroelastic system can be computed by the superposition of their respective modal solutions at each time step.

Received 23 July 2002; revision received 15 February 2003; accepted for publication 15 April 2003.

*Vice President, 7430 East Stetson Drive, Suite 205. Member AIAA.
†Engineering Specialist. Member AIAA.

II. Formulation

The basic assumption of the discrete time-domain state-space approach is that the nonlinearities in the aeroelastic system are measurable using a set of system parameters, called the nonlinear parameters, which are defined as $V_i(\xi)$, $i = 1, 2, \ldots, n$, where n is the number of the nonlinear parameters. Any response of the system such as the displacements, velocities, or acceleration at structural grid points, structural element forces, component loads, sensor output, actuator input, etc., can be defined as the nonlinear parameters. This leads to the following equation for the nonlinear aeroelastic system expressed as a function of multiple nonlinear parameters:

$$[M_{hh}(V_1, V_2, \ldots, V_n)]\{\ddot{\xi}\} + [B_{hh}(V_1, V_2, \ldots, V_n)]\{\dot{\xi}\} + [K_{hh}(V_1, V_2, \ldots, V_n)]\{\xi\} = \boldsymbol{P}_h(V_1, V_2, \ldots, V_n) + P_0 \quad (1)$$

where M_{hh}, B_{hh}, and K_{hh} are the generalized mass damping and stiffness matrices, respectively. $\boldsymbol{P}_h$ is the unsteady aerodynamic force vector, P_0 represents the gravitation and trim forces, and ξ are the generalized coordinates.

It can be seen that Eq. (1) is, in fact, the equation of motion of linear aeroelastic systems except that all of the aeroelastic system matrices in Eq. (1) are the function of the nonlinear parameters V_i. This suggests that if the relationships between M_{hh}, B_{hh}, K_{hh}, $\boldsymbol{P}_h$, and the nonlinear parameters V_i are given, these system matrices can be generated at a set of distinct values of V_i. For instance, for m distinct values of each V_i, this yields $m \times n$ sets of system matrices that correspond to $m \times n$ distinct values of the nonlinear parameters, denoted as $\bar{V}_{ij}$, $i = 1, 2, \ldots, n$, and $j = 1, 2, \ldots, m$. At each $\bar{V}_{ij}$, it is assumed that the aeroelastic system is locally linear, that is, M_{hhij}, B_{hhij}, K_{hhij}, and $\boldsymbol{P}_{hij}$ are constant. This gives an $m \times n$ set of state-space equations for the open-loop aeroelastic system:

$$\{\dot{X}_{ae}\} = [A_{ae}]_{ij}\{X_{ae}\} + [B_{ae}]_{ij}\{u_{ae}\} \quad (2)$$

where X_{ae} contains the structural and aerodynamic states and u_{ae} contains the deflection, rate, and acceleration vectors of the control surfaces. Here, the subscript ae denotes the aeroelastic system.

The outputs of the aeroelastic system are sensor readings whereas the inputs are the actuator servo commands. The sensor dynamics

and actuator dynamics also can be nonlinear and can be defined by the nonlinear parameters.

Combining the sensor and actuator dynamics with Eq. (2) yields an $m \times n$ set of state-space equations for the plant, that is,

$$\{\dot{X}_p\} = [A_p]_{ij}\{X_p\} + [B_p]_{ij}\{u_p\}, \qquad \{Y_p\} = [C_p]_{ij}\{X_p\} \quad (3)$$

where

$$[A_p] = \begin{bmatrix} A_{ae} & B_{ae} \\ 0 & A_{ac} \end{bmatrix}, \qquad [B_p] = \begin{bmatrix} 0 \\ B_{ac} \end{bmatrix}$$

$$[C_p] = [C_{ae} \quad D_{ae}], \qquad \{X_p\} = \begin{Bmatrix} X_{ae} \\ X_{ac} \end{Bmatrix} \quad (4)$$

and u_p and Y_p are the inputs and outputs of the plant, respectively. The subscripts p and ac in Eqs. (3) and (4) denote the plant and actuator, respectively.

The closed loop system can be obtained by connecting the plant with the control system through a gain matrix $[G]$. Note that variable gain matrices can be introduced as functions of the nonlinear parameters. The resulting closed-loop state-space equations are then transformed into an $m \times n$ set of discrete time-domain state-space equations shown as follows:

$$\{X\}_{k+1} = [\bar{A}]_{ij}\{X\}_k + [\bar{B}]_{ij}\{u\}_k \quad (5)$$

where k is the index of the time increments; $\{X\}$ is the state vector containing the structural states, the aerodynamic states, the actuator state, and the control system states; and $\{u\}$ is the external disturbance due to the pilot's input command or the discrete gust. Apparently, at each $\bar{V}_{ij}$, the construction of $[\bar{A}]_{ij}$ and $[\bar{B}]_{ij}$ from the aeroelastic and plant system matrices $[A_{ae}]$, $[B_{ae}]$, $[A_p]$, $[B_p]$, and $[C_p]$ is a standard industrial practice. For instance, such a procedure has been outlined by Hoadley and Karpel.[20] Note that if the discrete gust is employed as the external disturbance, the matrix $[\bar{B}]$ can be obtained based on the procedure presented in Ref. 21.

At each time step during the time-integration computation, the values of $V_i(\xi)$ are also calculated. Based on the values of $V_i(\xi)$, $[\bar{A}]$ and $[\bar{B}]$ matrices are updated by an interpolation scheme through the $m \times n$ set of $[\bar{A}]_{ij}$ and $[\bar{B}]_{ij}$. These updated $[\bar{A}]$ and $[\bar{B}]$ matrices are used for computing the transient solution of the next time step. The detailed solution procedure is discussed in the following section.

III. Solution Procedure

Figure 1 shows a block diagram of the solution procedure of the discrete time-domain state-space approach. This solution procedure can be generally divided into two parts, the preface phase and the time-integration computation.

In the preface phase, the system matrices K_{hhij}, M_{hhij}, B_{hhij}, and Q_{hhij} are first imported externally for each nonlinear parameter $\bar{V}_{ij}$. Next, the discrete time-domain $\bar{A}_{ij}$ and $\bar{B}_{ij}$ matrices associated with each $\bar{V}_{ij}$ are computed using the procedure presented in Ref. 20. The final step of the preface phase is to store $\bar{A}_{ij}$ and $\bar{B}_{ij}$ matrices on the run-time database.

To start the time-integration computation for transient response, it is required to specify the initial condition in terms of the trim solution. This trim solution can be obtained by performing a static aeroelastic analysis. One part of the trim solution is the generalized coordinate $\{\xi\}$ that is used as the initial values of ξ at $t = 0$ for the time-integration computation. In addition, the external disturbance can be defined either using the pilot's input command or the discrete gust. At each time step during the time integration computation, the values of the nonlinear parameters $V_i(\xi)$ are computed. These values are used to obtain $\bar{A}$ and $\bar{B}$ matrices by the interpolation through $\bar{A}_{ij}$ and $\bar{B}_{ij}$ matrices that are retrieved from the run-time database. The $\bar{A}$ and $\bar{B}$ matrices are then used as the system matrices of the discrete time-domain state-space equation to compute the transient solution of the next time step. Meanwhile, the transient solution of other parameters of interest such as component loads, element forces, grid point accelerations, etc., can be computed by superimposing their respective modal values with the solutions of the generalized coordinates. The time-integration computation terminates when it reaches its final values.

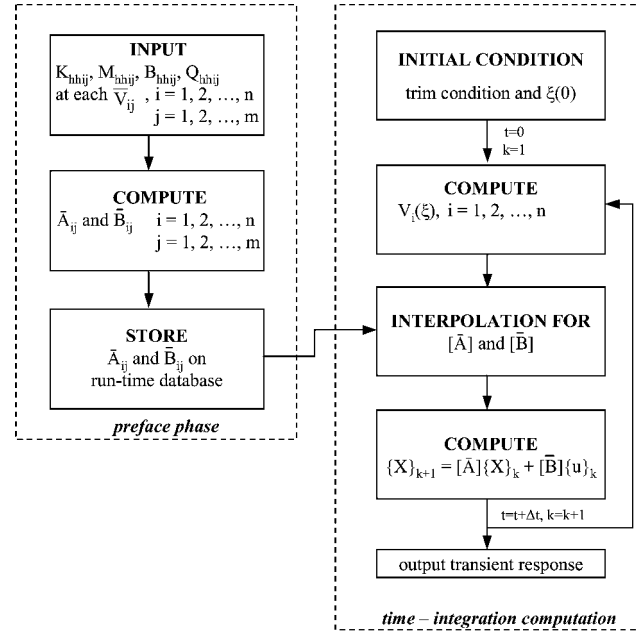

Fig. 1 Solution procedure of the discrete time-domain state-space approach.

IV. Issues of Modal Approach for Nonlinear Aeroelastic Systems

Equation (1) is derived based on the modal approach in which the physical coordinate $\{h\}$ is expressed in terms of the generalized coordinate $\{\xi\}$ through the lower-order normal modes of the structure $[\phi]$, that is,

$$\{h\} = [\phi]\{\xi\} \quad (6)$$

For linear aeroelastic analysis, the modal approach is a standard practice. However, for nonlinear aeroelastic analysis, Eq. (6) gives rise to an immediate technical issue regarding the selection of one set of modes that can best represent the physical coordinates in the entire nonlinear response domain. For instance, control surface with freeplay in the pitch degree of freedom can experience an abrupt change of the shape of the deformation when the pitch degree of freedom reaches the freeplay values, from a rigid-body pitch deformation to a clamped torsion deformation. Apparently, neither the modes of the control surface with free–free pitch degree of freedom nor with the clamped degree of freedom alone can be superimposed to represent accurately both the rigid-body pitch deformation and the clamped-torsion deformation simultaneously.

To circumvent this technical issue, it is recommended that the fictitious mass method described in Ref. 22 be employed to produce normal modes as the generalized coordinates in the nonlinear aeroelastic analysis. The objective of the fictitious mass method is to obtain a set of low-order modes by adding masses at the proper structural grid points so that the superimposed deformation from this set of modes can accurately represent the physical displacement. The natural frequencies of this structure with the added masses, of course, are different from those of the baseline structure. However, these added masses can be removed from the generalized mass matrix, rendering a system whose structural characteristics are practically identical to the baseline structure but with different mode shapes. For the control surface with freeplay case discussed, the best normal modes that can accurately represent both the rigid-body pitch deformation and the clamped-torsion deformation are those of the structures with free–free pitch degree of freedom but with a large mass attached to the pitch degree of freedom. This type of structure can produce a rigid-body pitch mode because of the

free–free pitch degree of freedom. However, it can also produce a mode that is nearly the same as the clamped-torsion mode because of the large mass at the pitch degree of freedom. Of course, this large mass should be removed after the modes are generated so that the natural frequencies of the structure remain nearly unaltered.

To verify that the selected normal modes can best represent the generalized coordinates of the nonlinear system, it is recommended to check the flutter speed of each sublinear system using the selected normal modes as the generalized coordinates to each of the sublinear system. The flutter speed of each sublinear system using this approach should not be significantly different than the flutter speed calculated using its own natural modes as the generalized coordinates.

V. Validation: Three-Degree-of-Freedom Airfoil Section with Freeplay Test Case

The three-degree-of-freedom (3-DOF) airfoil with freeplay test case is a typical airfoil section with control surface freeplay in incompressible flow whose transient response was obtained by Conner et al.[3] both numerically and experimentally. Figure 2 shows the structural system of such airfoil section that consists of 3-DOF, namely, the plunge h, the pitch α, and the flap β DOF. A ± 2.12 deg of freeplay is introduced in the control surface hinge point, which results in a restoring moment diagram shown in Fig. 3.

The equations of motion of the above 3-DOF airfoil with freeplay system can be expressed in the following equations:

$$[\bar{M}]\{\ddot{\xi}\} + [\bar{B}]\{\dot{\xi}\} + [\bar{K}]\{\xi\} + \lambda\{\bar{M}_\beta\} = q_\infty[\bar{Q}]\{\xi\} \tag{7}$$

where

$$[\bar{M}] = \begin{bmatrix} 3.293 & 0.0859 & 0.0039 \\ 0.0859 & 0.0135 & 0.0008 \\ 0.0039 & 0.0008 & 0.000326 \end{bmatrix}$$

is the generalized mass matrix,

$$[\bar{B}] = \begin{bmatrix} 3.29618 & 0.03517 & -0.0000356 \\ 0.03517 & 0.03042 & 0.00202 \\ -0.0000356 & 0.00202 & 0.0007757 \end{bmatrix}$$

is the generalized damping matrix, and

$$[\bar{K}] = \begin{bmatrix} K_h & 0 & 0 \\ 0 & K_\alpha & 0 \\ 0 & 0 & K_\beta \end{bmatrix}$$

is the generalized stiffness matrix without freeplay, where

$$K_h = 2818.8, \qquad K_\alpha = 37.3, \qquad K_\beta = 3.9$$

Here, $q_\infty[\bar{Q}]$is the time-domain generalized aerodynamic force matrix, q_∞ is the dynamic pressure, and $\{\xi\}^T = \{-h, \alpha, \beta\}$ are the generalized coordinates, where $-h$ denotes that the vertical displacement is positive upward and β is the relative deflection angle between the airfoil and the control surface.

The vector $\lambda\{\bar{M}_\beta\}$ in Eq. (7) represents the nonlinear structural effects due to freeplay, where λ is a switching parameter for the freeplay nonlinearity defined as

$$\begin{aligned} \lambda = -1 \quad &\text{for} \quad |\beta| \le \delta_0 \\ 0 \quad &\text{for} \quad |\beta| > \delta_0 \end{aligned} \tag{8}$$

where $\delta_0 = 2.12$ is the freeplay angle,

$$\{\bar{M}_\beta\} = \begin{bmatrix} 0 & & \\ & 0 & \\ & & K_\beta \end{bmatrix} \begin{Bmatrix} 0 \\ 0 \\ \beta \end{Bmatrix} + \begin{Bmatrix} 0 \\ 0 \\ M_0 \end{Bmatrix} \tag{9}$$

$$\begin{aligned} M_0 = -K_\beta\delta_0 \quad &\text{for} \quad \beta > 0 \\ K_\beta\delta_0 \quad &\text{for} \quad \beta < 0 \end{aligned}$$

M_0 is an offset moment. It is included so that the restoring moment in Fig. 3 does not pass through the origin.

The experiment of the 3-DOF airfoil with freeplay system was conducted in a low-speed wind tunnel with airspeed ranging from 4.3 to 24 m/s. Conner et al.[3] present excellent agreement between their wind-tunnel measurements and numerical results. This indicates that the experimental data are high quality and the structural data

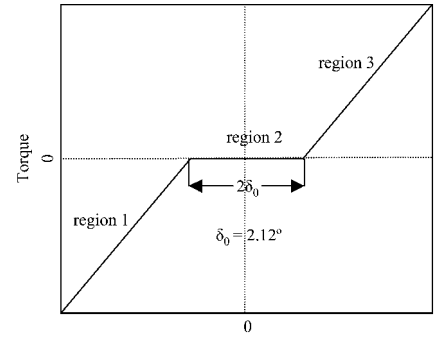

Fig. 3 Restoring moment diagram due to freeplay; relative deflection angle between airfoil and control surface, β.

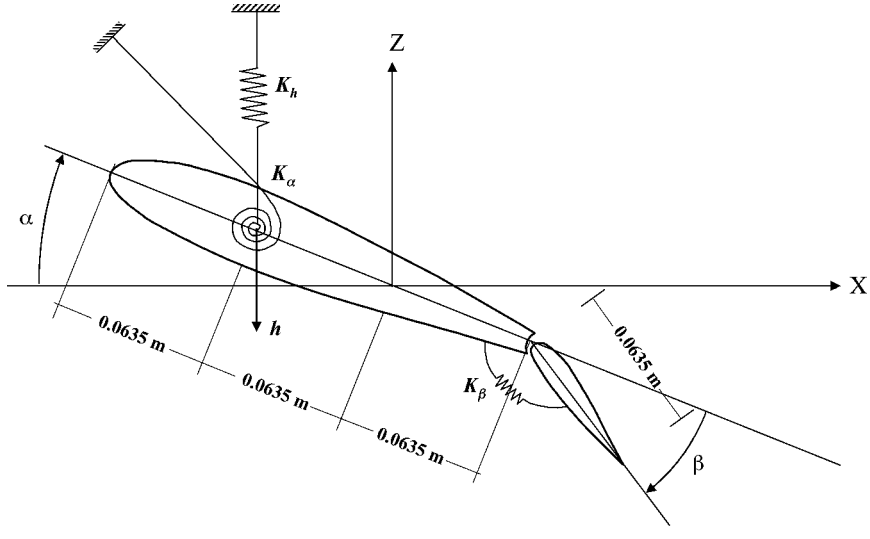

Fig. 2 Freeplay in 3-DOF airfoil.

presented earlier is of high accuracy. Therefore, this 3-DOF airfoil with freeplay system can be considered as a standard benchmark case for validating nonlinear aeroelastic methodologies.

In Ref. 3, the two-dimensional time-domain unsteady aerodynamics is generated using the Peters and Cao finite-state model.[23] In the present work, the unsteady aerodynamics is obtained on a high-aspect ratio rectangular wing shown in Fig. 4 using the three-dimensional frequency-domain unsteady aerodynamic method ZONA6.[24] Only the unsteady pressures along the root of the wing are selected so that the resulting unsteady aerodynamic forces are nearly two dimensional. This is verified by comparison with the Sears function shown in Fig. 5, where excellent agreement can be seen.

These ZONA6-generated two-dimensional frequency-domain, unsteady aerodynamics are then transformed into a time-domain rational function form using the Roger's approximation method.[25]

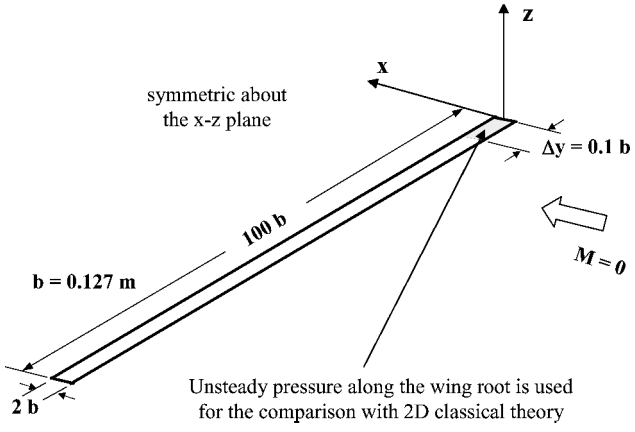

Fig. 4 High-aspect-ratio wing for two-dimensional aerodynamics.

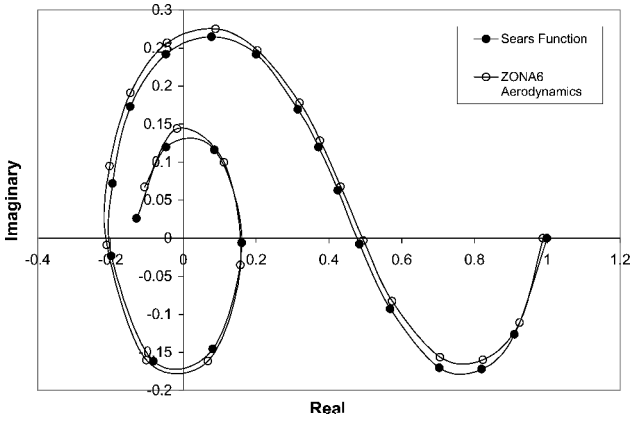

Fig. 5 Comparison of generalized aerodynamic forces between Sears function and ZONA6.

To verify the accuracy of the rational function approximation, the flutter speeds and frequencies of the linear 3-DOF airfoil aeroelastic system (without freeplay) at various K_β are computed by solving the eigenvalues of the open-loop state-space matrices and compared to those obtained by Tang et al.[2] This comparison is presented in Fig. 6. Good correlation between these two sets of results can be seen except that the present method predicts an abrupt change in the flutter frequency from high to low at $K_\beta \approx 1.2$ N, which is slightly lower than that presented by Tang et al.[2] This is probably caused by the difference in unsteady aerodynamics computed by ZONA6 and the Peters and Cao[23] finite-state methods.

Based on the restoring moment diagram shown in Fig. 3, three sets of state-space equations are generated using the stiffness matrices and the offset moments corresponding to regions 1–3 shown in Fig. 3. The flap rotation angle β is defined as the nonlinear parameter whose solution at each time step is used to determine the state-space equations of the next time step. To excite the nonlinear system, a one-cycle flap oscillation with various amplitudes is introduced at the initial time. The objective of using various amplitudes is to study the impact of initial disturbance on the response of the nonlinear system.

Note that in both the Conner et al.[3] experimental and numerical results of the 3-DOF airfoil section with freeplay, five types of motion were observed during the transition of the nonlinear responses from low airspeeds to high airspeeds. These five types of motion are classified as damped decay (convergent motion), periodic limit-cycle oscillation [(LCO) with nonharmonic periodicity], intermittent chaos (randomlike motion in completely deterministic nonlinear systems), nearly harmonic LCO (LCO with harmonic motion), and flutter (divergent motion). The predictability for these five types of motion using the present discrete time-domain state-space approach is presented in Fig. 7.

In Fig. 7, the root-mean-square amplitudes of the pitch, plunge, and flap motions and the steady-state frequency in various airspeeds obtained by the Conner et al.[3] experiment and numerical analysis and by the present approach are shown. At low airspeeds (below $U/U_f = 0.18$, where $U_f = 23.9$ m/s is the flutter speed without freeplay), the transient response is the damped decay-type of motion, which is independent of the initial disturbance. When the airspeed increases up to $U/U_f = 0.35$, the transient response becomes a periodic type of LCO with a low steady-state frequency slightly below 5 Hz. It is also observed both experimentally and numerically that this periodic LCO is sensitive to the initial disturbance, that is, LCO is obtained only if the amplitude of the one-cycle flap oscillation is sufficiently large. When the airspeed is in the neighborhood of $U/U_f = 0.5$, the low-frequency LCO becomes unstable and loses its periodicity. This type of motion was defined earlier as intermittent chaos-type of motion, that is, periodicity can be observed only after long periods of oscillation. When the airspeed is further increased beyond $U/U_f = 0.55$, the transient response abruptly changes to a nearly harmonic LCO with a dominated frequency around 11 Hz, which was classified earlier as the nearly harmonic LCO. Note that this nearly harmonic LCO is insensitive to the initial disturbance. When the airspeed reaches $U/U_f = 1$, of

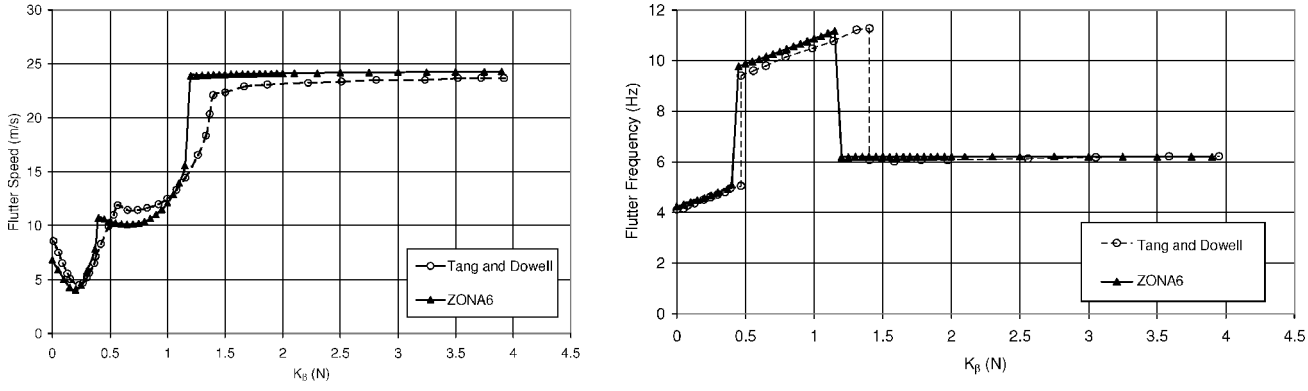

Fig. 6 Linear flutter speed and frequency vs K_β of the 3-DOF airfoil section.

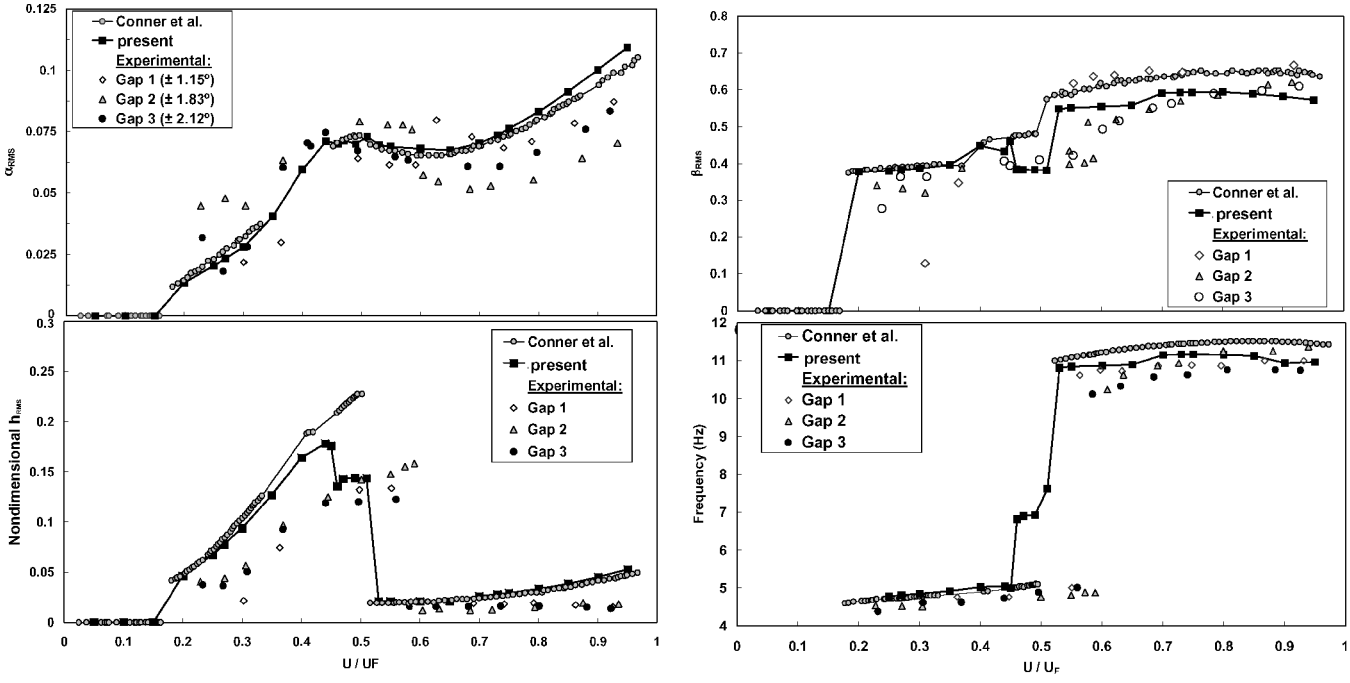

Fig. 7 Root-mean-square amplitudes at various airspeeds.

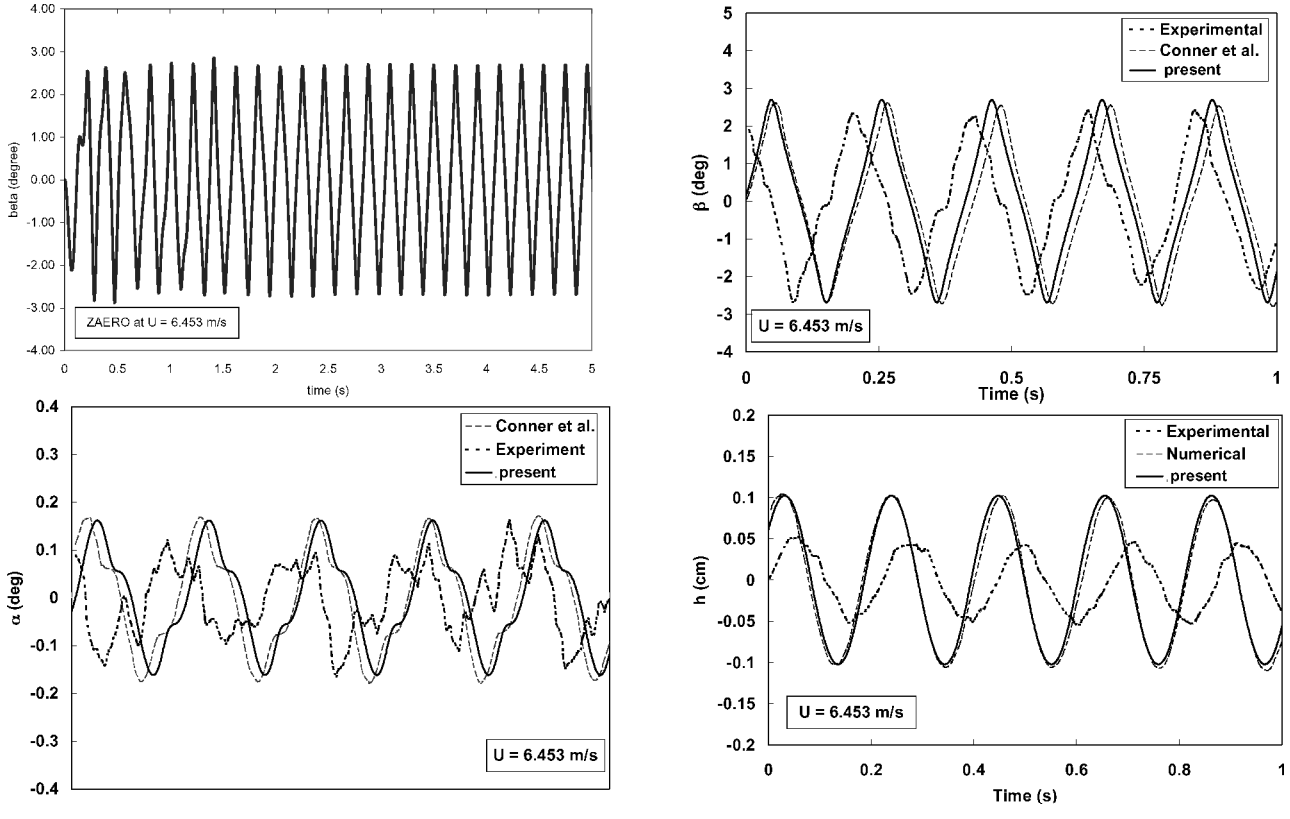

Fig. 8 Transient responses of 3-DOF airfoil with freeplay at $U = 6.453$ m/s.

course, divergent flutter occurs. The transient responses of the periodic LCO, intermittent chaos, and nearly harmonic LCO obtained by the present approach and the Conner et al.[3] experiment and numerical analysis at $U/U_f = 0.27$, 0.43, and 0.74 are presented in Figs. 8, 9, and 10, respectively.

Note that the results obtained by the present approach agree very well with the Ref. 3 numerical results. Furthermore, both methods predict the qualitative and quantitative behavior found experimentally fairly accurately except for the plunge motion, where both methods slightly overpredict the amplitude.

VI. Application: Strut-Braced Wing Subjected to a Discrete Gust

The strut-braced wing concept proposed by the Virginia Polytechnic Institute and State University team[26] is designed based on a multidisciplinary design optimization approach for a higher aerodynamic efficiency and a lower structural weight. Figure 11 shows the geometry of the strut-braced wing (SBW) whose structure is obtained by a fully stressed design. To avoid strut buckling, a telescoping sleeve mechanism to disengage strut during the negative-gravitationalacceleration maneuvers was proposed.[26]

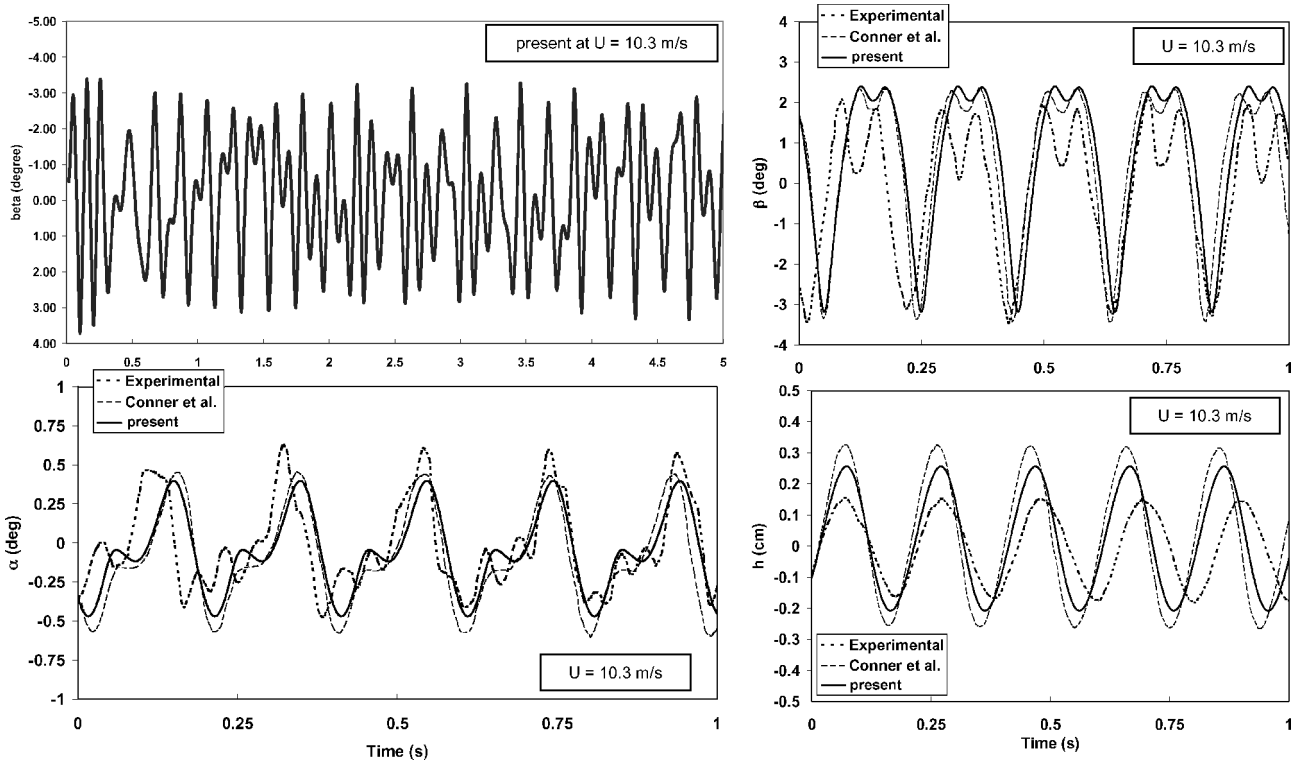

Fig. 9 Transient responses of 3-DOF airfoil with freeplay at $U = 10.3$ m/s.

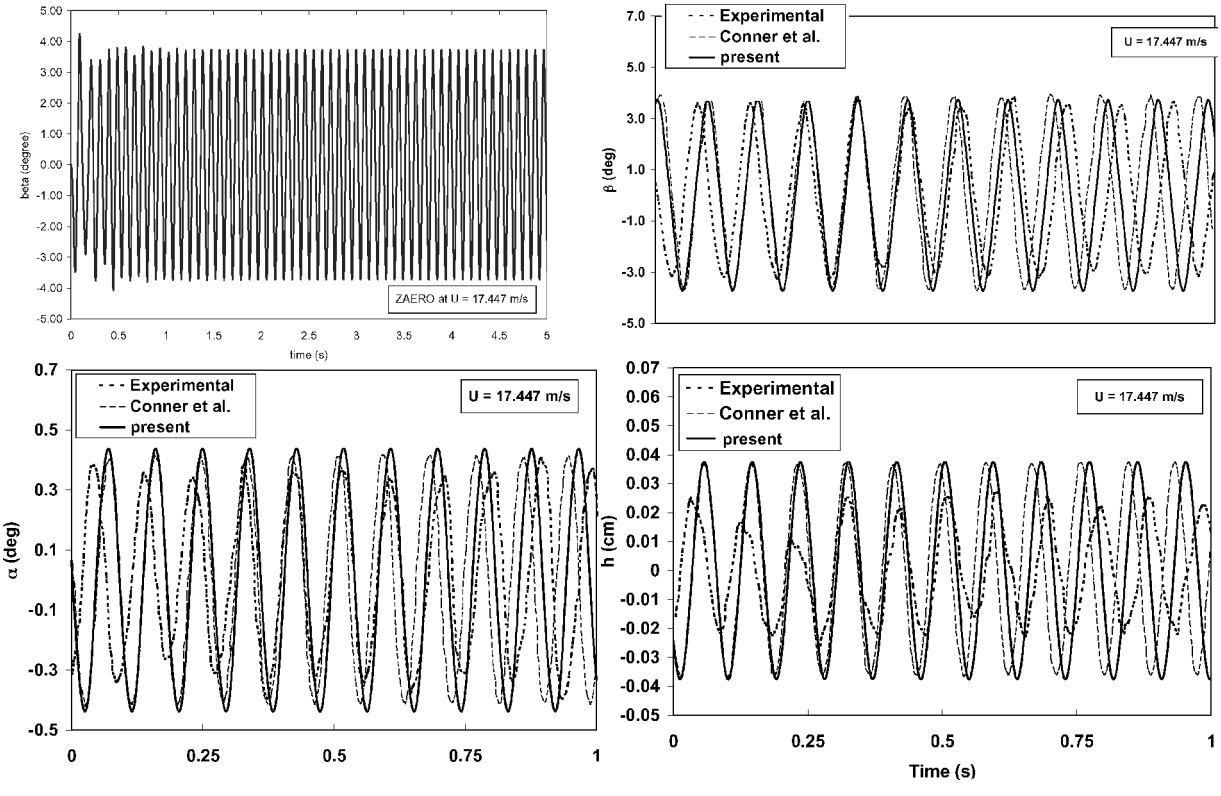

Fig. 10 Transient responses of 3-DOF airfoil with freeplay at $U = 17.447$ m/s.

In the present study, a similar SBW configuration, but without the telescoping sleeve mechanism, is used. Apparently the fully stressed design does not warrant the aeroelastic stability of the structure, particularly if the buckling of the wing or strut occurs. Linear buckling analysis shows that the axial buckling forces of the wing and the strut are $P_{\text{wing}} = 9.34 \times 10^6$ N and $P_{\text{strut}} = 5.60 \times 10^5$ N, respectively. Table 1 presents the natural frequencies and the flutter speeds/frequencies at $M = 0.53$ of the nominal structure, strut-buckled structure and the wing-buckled structure. Note that the residual stiffness of the strut-buckled structure is assumed to be 10% of its nominal stiffness.

The designed cruise condition of the SBW aircraft is at $M = 0.53$ and airspeed = 198 m/s, which is beyond the flutter speeds of the strut-buckled and wing-buckled structures. This suggests that the SBW could encounter flutter instability if either the strut or the wing buckles.

Table 1 Aeroelastic characteristics of SBW at $M = 0.53$

Structure	First/second natural frequencies, Hz	Flutter speed, m/s (flutter frequency, Hz)	
		Direct method	Use strut-buckled modes
Nominal	2.08/2.79	247 (3.94)	251 (3.92)
Strut buckled	1.93/2.11	170 (3.75)	170 (3.75)
Wing buckled	0.70/1.95	Very low	Very low

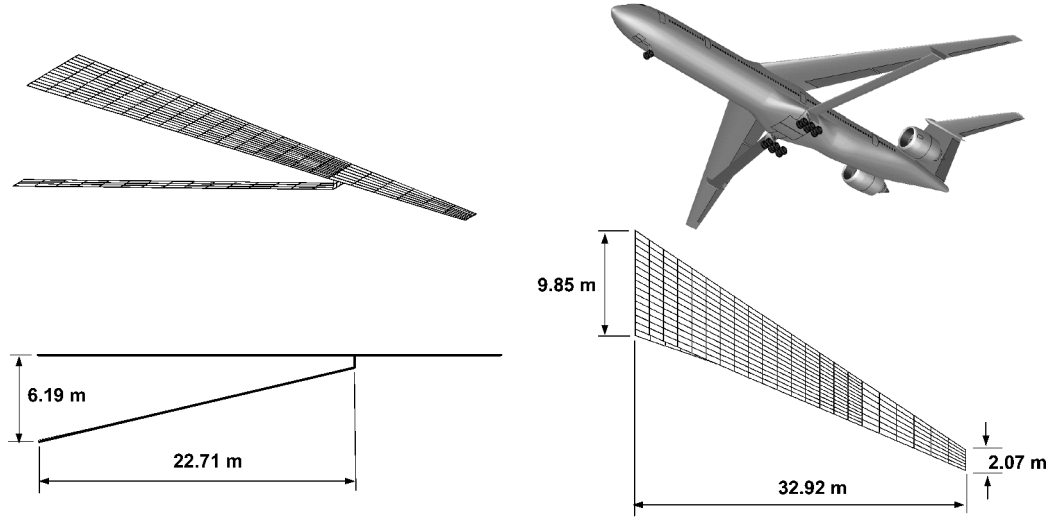

Fig. 11 Geometry of SBW.

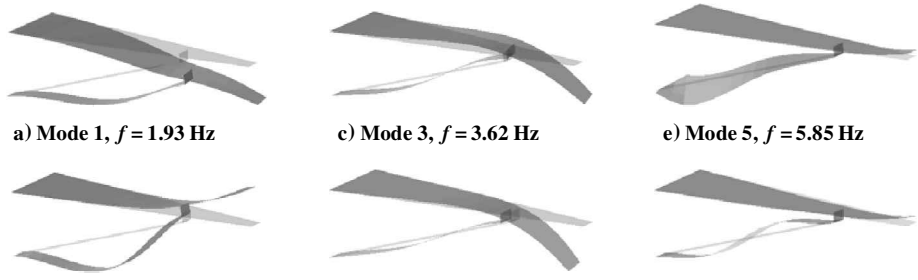

a) Mode 1, $f = 1.93$ Hz **c) Mode 3, $f = 3.62$ Hz** **e) Mode 5, $f = 5.85$ Hz**

b) Mode 2, $f = 2.11$ Hz **d) Mode 4, $f = 3.88$ Hz** **f) Mode 6, $f = 6.06$ Hz**

Fig. 12 First six mode shapes of strut-buckled structures.

Generally, there are two types of loads that could buckle the SBW structure; the static trim loads at an extreme maneuver condition and the dynamic loads due to a discrete gust. Two extreme maneuver conditions are selected for the present analysis, a 2.5-g trim condition and a -1-g trim condition. According to the Federal Air Regulation 25 for the discrete gust design criteria, a $1-$ cosine 25 chord gust with gust velocity $W_g = 15.24$ m/s is used to induce the dynamic loads on the SBW structure. The trim solutions are obtained by performing a static aeroelastic analysis that provides the trim angles of attack of 7.155 deg for the 2.5-g trim condition and -2.86 deg for the -1-g trim condition. The aerodynamic and inertial loads at these two trim conditions are then combined with the gust loads used as the external forces applied on the SBW. Note that there is a 1-s delay (gust reference point ahead of the wing by 198 m) introduced to the $1-$ cosine gust profile. This is to exclude the gust loads at the initial time so that the transient response in the first 1 s is purely due to the trim loads.

As already discussed, one of the technical issues in nonlinear aeroelastic analysis is how to select one set of mode shapes that can best represent the structural deformations at various nonlinear regions. For the SBW case, it is found that the first 20 modes of the strut-buckled structure are capable of representing the structural deformations of the nominal as well as the wing-buckled structures accurately. This is verified by performing the flutter analysis for the nominal structure and the wing-buckled structures but using the mode shapes of the strut-buckled structure as the generalized coordinates. Excellent agreement in terms of flutter speed with those presented in Table 1 is obtained, verifying that the mode shapes of the strut-buckled structure are the good choice as the generalized coordinates of the nonlinear aeroelastic analysis for the SBW structure. The first six mode shapes of the strut-buckled structure and the corresponding natural frequencies are shown in Fig. 12.

The axial forces along the strut, P_{strut}, and the wing, P_{wing}, are selected as the two nonlinear parameters that divide the nonlinear system into locally linear systems shown as follows.

Nominal structure:

$$-\infty < P_{\text{strut}} < 5.60 \times 10^5 \text{ N}$$

Strut-buckled structures:

$$5.60 \times 10^5 \text{ N} \leq P_{\text{strut}} < \infty$$

Nominal structure:

$$-\infty < P_{\text{wing}} < 9.34 \times 10^6 \text{ N}$$

Wing-buckled structure:

$$9.34 \times 10^6 \text{ N} \leq P_{\text{wing}} < \infty$$

This leads to four sets of state-space equations. The switching of the time integration among these four sets of state-space equation is determined by the nonlinear parameters P_{strut} and P_{wing}. At each

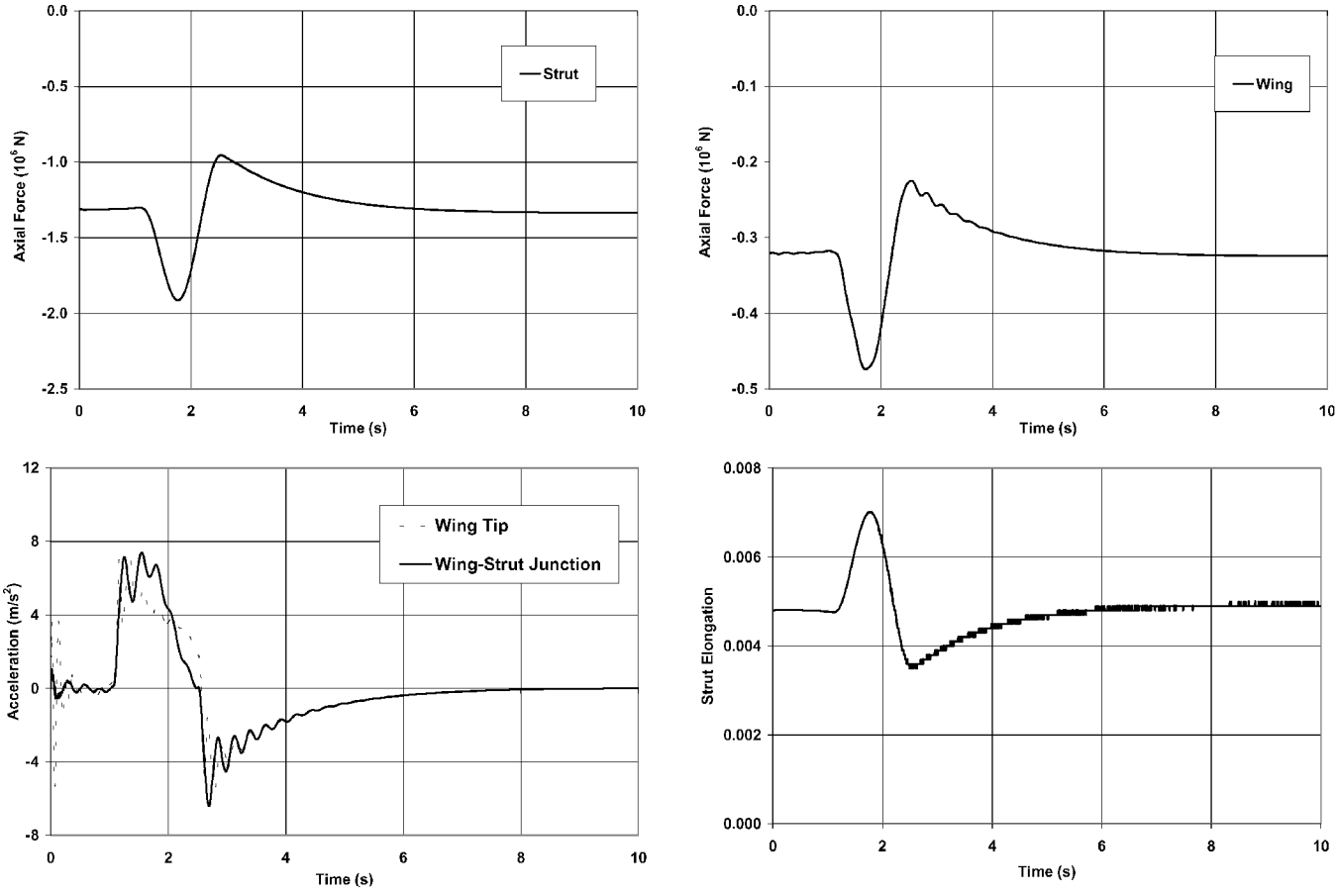

Fig. 13 Transient responses of SBW at 2.5-*g* trim condition.

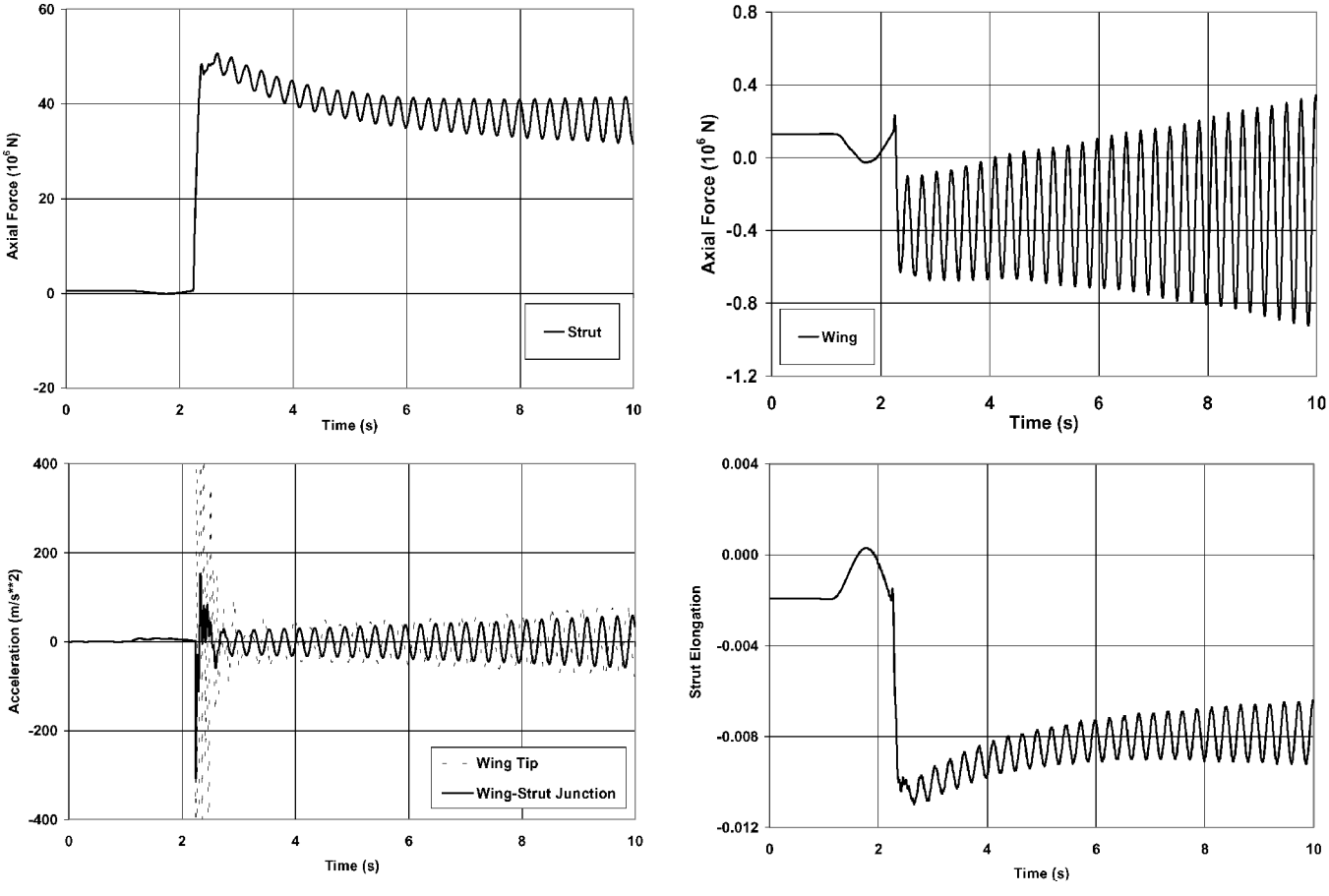

Fig. 14 Transient response of SBW at −1-*g* trim condition.

time step, after the solution of the generalized coordinate $\xi(t)$ is computed, P_{strut} and P_{wing} can be obtained by the following equation:

$$P(t) = [K_{\text{nominal}}][\varphi_{\text{strut-buckled}}]\{\xi(t)\} \tag{10}$$

where K_{nominal} is the stiffness matrix of the nominal structure and $\varphi_{\text{strut-buckled}}$ is the modal matrix of the strut-buckled structure. In Eq. (10), the selection of the stiffness matrix of the nominal structure is due to the fact that the axial buckling forces of the strut and the wing are computed based on the nominal structure.

Before the time integration is started, the discrete time-domain $\bar{A}_{ij}$ and $\bar{B}_{ij}$ matrices associated with the four locally linear subsystems were stored on a run-time database. The database includes also the strut-buckled modes as the generalized coordinates for each locally linear subsystem. Based on this strategy, there is no need to update the structural modes for each time steps, and therefore, this reduces the computational time considerably.

The time-integration computation for the nonlinear transient response is performed from $t = 0$ to 10 s with a time step of 0.001 s. At each time step, the axial forces along the strut and the wing, vertical accelerations at the wing tip, and the wing–strut junction as well as the strut elongation are computed. These transient responses are then used to determine the stability of the SBW with different externally loads conditions.

The transient responses of the SBW subjected to the 1− cosine gust at 2.5-g trim condition are presented in Fig. 13. It can be seen that throughout the time history neither the wing axial force nor the strut axial force exceeds their respective buckling forces ($P_{\text{wing}} = 9.34 \times 10^6$ N and $P_{\text{strut}} = 5.60 \times 10^5$ N), which implies that the structure remains at the nominal state throughout the entire time-integration computation. Because the airspeed at $V = 198$ m/s is below the flutter speed of the nominal structures ($U_f = 251$ m/s), the aeroelastic system is stable. Therefore, once the SBW passes through the 1− cosine gust profile, damped decay motion occurs and converges to the initial trim values.

When the SBW is at the −1-g trim condition, the transient responses shown in Fig. 14 become drastically different from those of the 2.5-g trim condition. At $t = 2.2$ s, the trim loads at −1-g condition combined with the gust loads "kick" the strut into its buckling state, that is, the axial force exceeds its buckling force ($P_{\text{strut}} = 5.60 \times 10^5$ N). Because the airspeed at 198 m/s is beyond the flutter speed of the strut-buckled structure ($U_f = 170$ m/s), after $t = 2.2$ s the structure becomes aeroelastically unstable and divergent response occurs.

The results of the 2.5-g and −1-g trim condition show that the stability of the present SBW configuration is trim condition dependent. Such results clearly can not be obtained by a linear aeroelastic analysis.

VII. Conclusions

There are many instances where nonlinear effects become crucial to an efficient and safe design of aeroservoelastic systems. Nonlinearities can exist in structures, aerodynamics, and control systems, for example, friction, geometric nonlinearity, freeplay, large-amplitude unsteady aerodynamics, and control saturation. To develop a general purpose simulation tool that can handle all types of nonlinearities is not likely.

Based on the nonlinear parameter scheme, the present method relies on externally imported system matrices, provided that the nonlinearities of these system matrices are measurable using the nonlinear parameter scheme, to assemble a set of discrete time-domain state-space equations. The overall transient response of the nonlinear system is then obtained by switching the time-integration procedure between these discrete time-domain state-space matrices. In so doing, various nonlinearities, if not all, can be included in the state-space equations. However, further studies are required to show the generality of the present method, ideally on a case involving structural, aerodynamic, and control system nonlinearities.

Acknowledgment

The authors thank D. M. Tang of Duke University for providing the structural data of the three-degree-of-freedom airfoil section with freeplay case.

References

[1]Tang, D., Kholodar, D., and Dowell, E. H., "Nonlinear Response of Airfoil Section with Control Surface Freeplay to Gust Loads," *AIAA Journal*, Vol. 38, No. 9, 2000, pp. 1543–1557.

[2]Tang, D., Dowell, E. H., and Virgin, L. N., "Limit Cycle Behavior of an Airfoil with a Control Surface," *Journal of Fluids and Structures*, Vol. 12, 1998, pp. 839–858.

[3]Conner, M. D., Tang, D. M., Dowell, E. H., and Virgin, L. N., "Nonlinear Behavior of a Typical Airfoil Section with Control Surface Freeplay: A Numerical and Experimental Study," *Journal of Fluids and Structures*, Vol. 11, 1997, pp. 89–109.

[4]Price, S. J., Alighanbari, H., and Lee, B. H. K., "The Aeroelastic Response of a Two-Dimensional Airfoil with Bilinear and Cubic Structural Nonlinearities," *Journal of Fluids and Structures*, Vol. 9, 1995, pp. 175–193.

[5]Price, S. J., Lee, B. H. K., and Alighanbari, H., "Postinstability Behavior of a Two-Dimensional Airfoil with a Structural Nonlinearity," *Journal of Aircraft*, Vol. 31, 1994, pp. 1395–1401.

[6]Murphy, K. D., Bayly, P. V., Virgin, L. N., and Gottwald, J. A., "Measuring the Stability of Periodic Attractors Using Perturbation-Induced Transients: Applications to Two Non-Linear Oscillators," *Journal of Sound and Vibration*, Vol. 172, 1994, pp. 85–102.

[7]Hauenstein, A. J., Zara, J. A., Eversman, W., and Qumei, I., "Chaotic and Nonlinear Dynamic Response of Aerosurfaces with Structural Nonlinearities," AIAA Paper 92-2547, April 1992.

[8]Brase, L. O., and Eversman, W., "Application of Transient Aerodynamics to the Structural Nonlinear Flutter Problem," *Journal of Aircraft*, Vol. 25, No. 11, 1988, pp. 1060–1068.

[9]Lee, C. L., "An Iterative Procedure for Nonlinear Flutter Analysis," *AIAA Journal*, Vol. 24, No. 5, 1986, pp. 833–840.

[10]Kousen, K. A., and Bendiksen, O. O., "Limit-Cycle Phenomena in Computational Transonic Aeroelasticity," *Journal of Aircraft*, Vol. 31, 1982, pp. 1257–1263.

[11]McIntosh, S. C., Jr., Reed, R. E., Jr., and Rodden, W. P., "An Experimental and Theoretical Study of Nonlinear Flutter," *Journal of Aircraft*, Vol. 18, Dec. 1981, pp. 1057–1063.

[12]Desmarais, R. N., and Reed, W. H., "Wing Store Flutter with Nonlinear Pylon Stiffness," AIAA Paper 80-0792, May 1980.

[13]Laurenson, R. M., and Trn, R. M., "Flutter of Control Surfaces with Structural Nonlinearities," *AIAA Journal*, Vol. 18, No. 10, 1980, pp. 1245–1251.

[14]Breitbach, E., "Flutter Analysis of an Airplane with Multiple Structural Nonlinearities in the Control System," NASA TP-1620, March 1980.

[15]Breitbach, E., "Effects of Structural Non-Linearities on Aircraft Vibration and Flutter," AGARD Rept. 665, Sept. 1977.

[16]Miller, M. Z., "Two Degree of Freedom Flutter Analysis Including Effects of Structural Nonlinearities," McDonnell Douglas Astronautics Corp., Rept. E2236-ATN—001, St. Louis, MO, Dec. 1972.

[17]Shen, S. F., "An Approximate Analysis of Nonlinear Flutter Problems," *Journal of Aero/Space Sciences*, Vol. 26, Jan. 1959, pp. 25–32, 45.

[18]Woolston, D. S., Runyan, H. L., and Andrews, R. E., "An Investigation of Effects of Certain Types of Structural Nonlinearities on Wing and Control Surface Flutter," *Journal of the Aeronautical Sciences*, Vol. 24, Jan. 1957, pp. 57–63.

[19]Greif, H. D., "Describing Function Method of Servomechanism Analysis Applied to Most Commonly Encountered Nonlinearities," *American Institute of Electrical Engineering Transactions–Pt. II: Applications and Industry*, Vol. 72, No. 8, 1953, pp. 243–248.

[20]Hoadley, S. T., and Karpel, M., "Applications of Aeroservoelastic Modeling Using Minimum-State Unsteady Aerodynamic Approximations," *Journal of Guidance, Control, and Dynamics*, Vol. 14, No. 6, 1991, pp. 1267–1276.

[21]Chen, P. C. "Nonhomogenous State-Space Approach for Discrete Gust Analysis of Open-Loop/Closed-Loop Aeroelastic Systems," AIAA Paper 2002-1715, April 2002.

[22]Karpel, M., and Presente, E., "Structural Dynamic Loads in Response to Impulsive Excitation," *Journal of Aircraft*, Vol. 32, No. 4, 1995, pp. 853–861.

[23]Peters, D. D., and Cao, W. M., "Finite State Induced Flow Models, Part 1: Two-Dimensional Thin Airfoil," *Journal of Aircraft*, Vol. 32, 1995, pp. 313–322.

[24]Chen, P. C., Lee, H. W., and Liu, D. D., "Unsteady Subsonic Aerodynamics for Bodies and Wings with External Stores Including Wake Effect," *Journal of Aircraft*, Vol. 30, No. 5, 1993, pp. 618–628.

[25]Roger, K. L., "Airplane Math Modeling and Active Aeroelastic Control Design," *Structural Aspects of Active Control*, CP-228, AGARD, 1977, pp. 4.1–4.11.

[26]Sulaeman, E., Kapania, R. K., and Haftka, R. T., "Effect of Compressive Force on a Strut-Braced Wing Response," AIAA Paper 2001-1611, April 2001.

E. Livne
Associate Editor